Results from muon reconstruction performance with ATLAS at Run-3

Andres Pinto on behalf of the ATLAS Collaboration

Université Paris-Saclay, CEA, Département de Physique des Particules, 91191, Gif-sur-Yvette, France.
Institut für Physik, Universität Mainz, 55122 Mainz, Germany.
andres.eloy.pinto.pinoargote@cern.ch

1. The ATLAS detector

Multipurpose particle detector with a forward–backward symmetric cylindrical geometry. It consists of an Inner Detector (ID) (left), electromagnetic and hadronic calorimeters, and a Muon Spectrometer (MS) (right). In Run3, the experimental setup has undergone enhancements through the replacement of the Small Whell by the New Small Wheel (NSW) and the implementation of updates in the muon trigger systems.

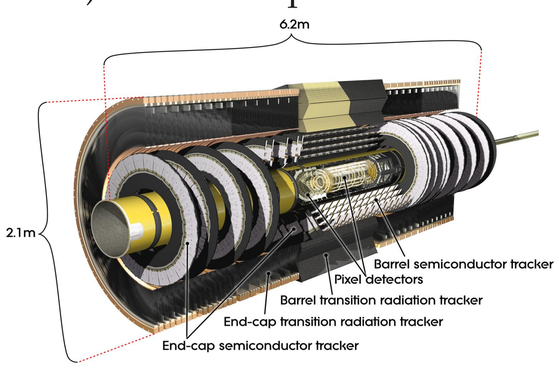

Inner Detector: track charged particle detector for $|\eta| < 2.5$ with a 2 [T] solenoid magnetic field.

Muon Spectrometer: muon tracking detector for $|\eta| < 2.7$ with a 0.6 [T] toroidal magnetic field with precision and trigger chambers.

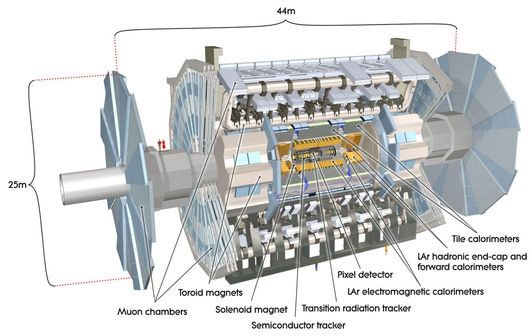

The ATLAS dataset taken at $\sqrt{s} = 13.6$ TeV in 2022 comprises an integrated delivered luminosity of $\approx 38.5\,\text{fb}^{-1}$.

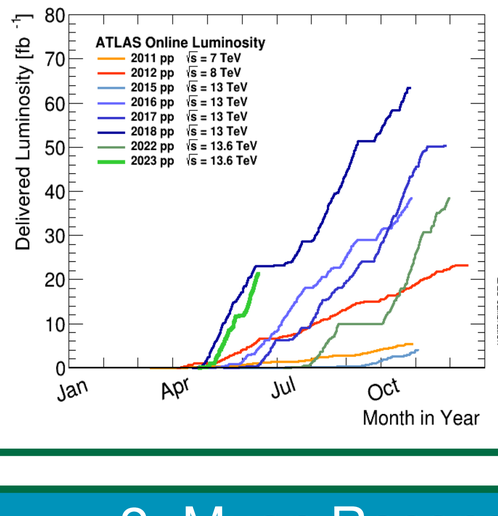

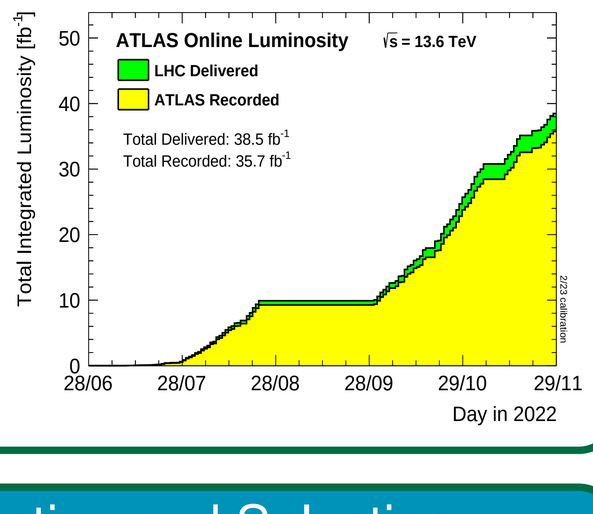

2. Muon Reconstruction and Selection

Muons are reconstructed by combining the ID and MS information giving the following types: Combined, Segment-tagged, Standalone and Calorimeter-tagged muons.

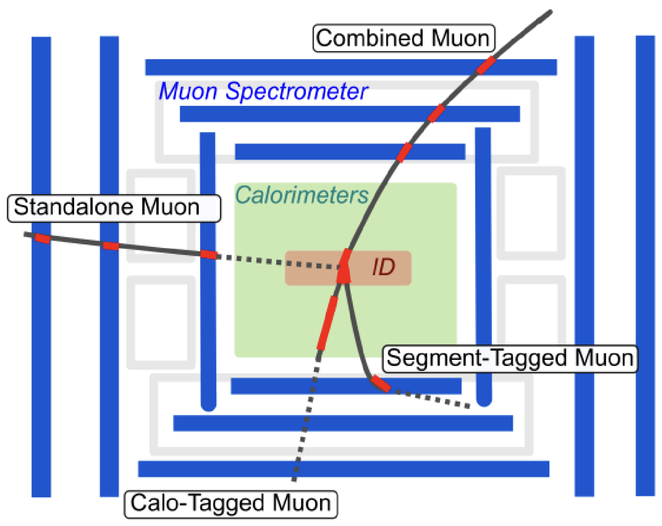

Two working points are defined according to purity level and kinematics:

- **Loose:** High efficiency but less purity and larger systematics.
- **Medium:** suitable efficiency and purity with low systematics.

Efficiency is determined in both data and simulation by the **Tag-and-Probe** method applied to $Z \to \mu\mu$ and $J/\psi \to \mu\mu$ described in **EPJC 81, 578 (2021)**. The deviation of the simulation from the detector behavior is estimated by a Scale Factor (efficiencies ratio) that is used to correct the simulation.

The Muon isolation is either track-based or calorimeter-based and defined as the transverse energy (or momentum if considering only tracks) reconstructed in a cone around a muon and divided by the muon p_T. Several working points are defined combining selections on track-based and calorimeter-based isolation that result in better performance.

Some of these working points use a particle-flow based algorithm to evaluate the neutral component of the energy deposit

3. Reconstruction and Isolation Efficiency

Top: Muon reconstruction and identification efficiency for $J/\psi \to \mu\mu$ as a function of η and p_T of the muon (left) and $Z \to \mu\mu$ as a function of φ and η (right).
Bottom: Isolation efficiency for $Z \to \mu\mu$ as a function of p_T of the muons for Tight (left) and PflowTight (right) quality criteria.

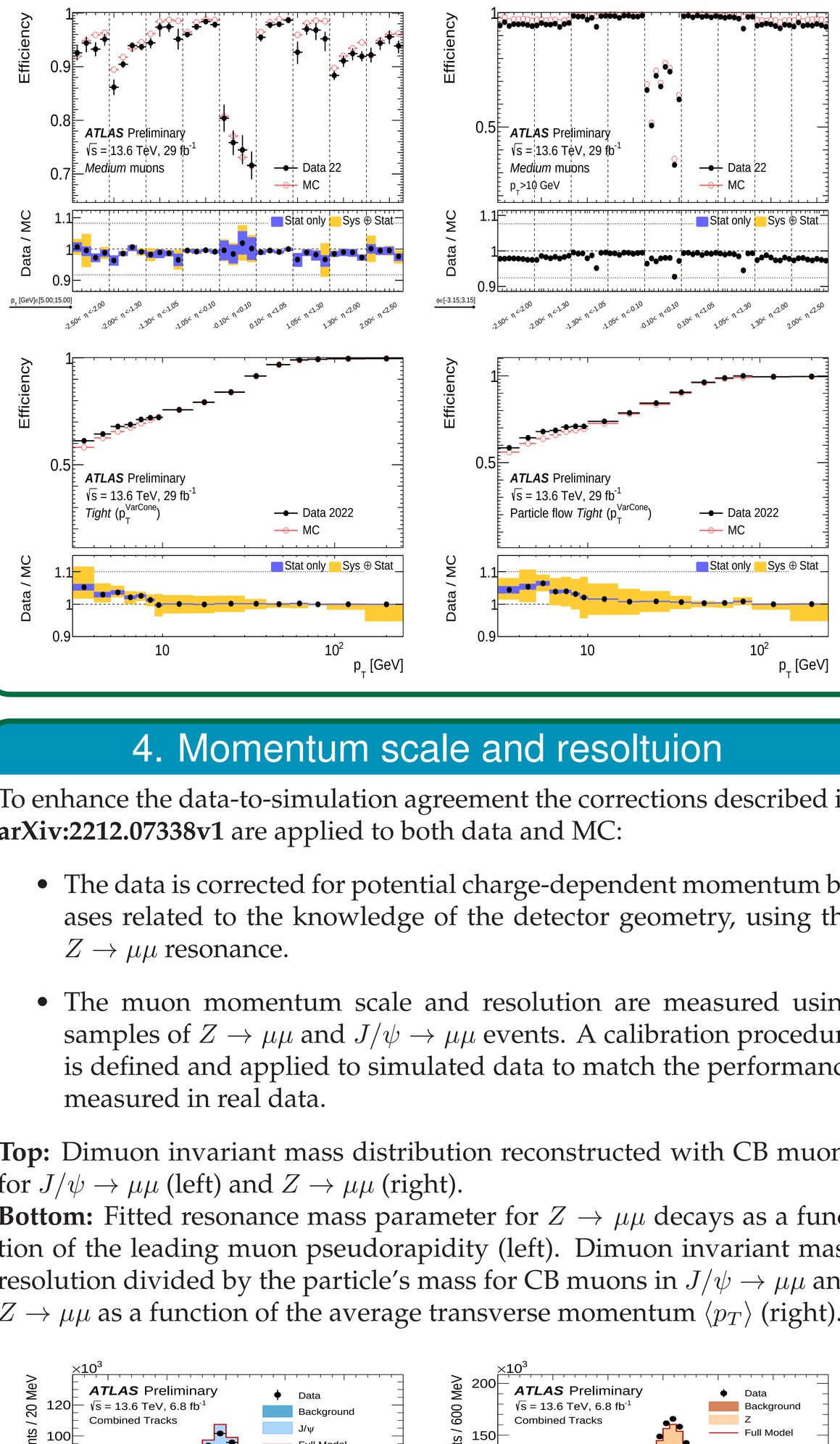

4. Momentum scale and resoltuion

To enhance the data-to-simulation agreement the corrections described in **arXiv:2212.07338v1** are applied to both data and MC:

- The data is corrected for potential charge-dependent momentum biases related to the knowledge of the detector geometry, using the $Z \to \mu\mu$ resonance.
- The muon momentum scale and resolution are measured using samples of $Z \to \mu\mu$ and $J/\psi \to \mu\mu$ events. A calibration procedure is defined and applied to simulated data to match the performance measured in real data.

Top: Dimuon invariant mass distribution reconstructed with CB muons for $J/\psi \to \mu\mu$ (left) and $Z \to \mu\mu$ (right).
Bottom: Fitted resonance mass parameter for $Z \to \mu\mu$ decays as a function of the leading muon pseudorapidity (left). Dimuon invariant mass resolution divided by the particle's mass for CB muons in $J/\psi \to \mu\mu$ and $Z \to \mu\mu$ as a function of the average transverse momentum $\langle p_T \rangle$ (right).